

Chapter 7

Heat

7.1 Introduction

Volcanoes, intrusions, earthquakes, mountain building and metamorphism are all controlled by the transfer and generation of heat. The Earth's thermal budget controls the activity of the lithosphere and asthenosphere as well as the development of the innermost structure of the Earth.

Heat arrives at the Earth's surface from its interior and from the Sun. Virtually all the heat comes from the Sun, as any sunbather knows, but is all eventually radiated back into space. The rate at which heat is received by the Earth, and re-radiated, is about 2×10^{17} W or, averaged over the surface, about 4×10^2 W m⁻². Compare this value with the mean rate of loss of internal heat from the Earth, 4.4×10^{13} W (or 8.7×10^{-2} W m⁻²); the approximate rate at which energy is released by earthquakes, 10^{11} W; and the rate at which heat is lost by a clothed human body on a very cold (-30°C), windy (10 m s^{-1}) Canadian winter day, 2×10^3 W m⁻². From a geological perspective, the Sun's heat is important because it drives the surface water cycle, the rainfall and, hence, erosion. However, the heat source for igneous intrusion, metamorphism and tectonics is within the Earth, and it is this internal source which accounts for most geological phenomena. The Sun and the biosphere have kept the surface temperature within the range of the stability of liquid water, probably $15\text{--}25^\circ\text{C}$ averaged over geological time. Given that constraint, the movement of heat derived from the interior has governed the geological evolution of the Earth, controlling plate tectonics, igneous activity, metamorphism, the evolution of the core and hence the Earth's magnetic field.

Heat moves by conduction, convection, radiation and advection. *Conduction* is the transfer of heat through a material by atomic or molecular interaction within the material. In *convection*, heat transfer occurs because the molecules themselves are able to move from one location to another within the material; it is important in liquids and gases. In a room with a hot fire, air currents are set up, which move the light, hot air upwards and away from the fire while dense cold air moves in. Convection is a much faster way of transferring heat than conduction. As an example, when we boil a pan of water on the stove, the heat is transferred through the metal saucepan by conduction but through the water primarily by convection.

Radiation involves direct transfer of heat by electromagnetic radiation (e.g., from the Sun or an electric bar heater). Within the Earth, heat moves predominantly by conduction through the lithosphere (both oceanic and continental) and the solid inner core. Although convection cannot take place in rigid solids, over geological times the Earth's mantle appears to behave as a very-high-viscosity liquid, which means that slow convection is possible in the mantle (see Sections 6.1, 7.4 and 8.2); in fact, heat is generally thought to be transferred by convection through most of the mantle as well as through the liquid outer core. Although hot lava radiates heat, as do crystals at deep, hot levels in the mantle, radiation is a minor factor in the transfer of heat within the Earth. *Advection* is a special form of convection. When a hot region is uplifted by tectonic events or by erosion and isostatic rebound, heat (called advected heat) is physically lifted up with the rocks.

It is not possible to measure temperatures deep in the Earth. Temperatures and temperature gradients can be measured only close to the Earth's surface, usually in boreholes or mines or in oceanic sediments. The deeper thermal structure must be deduced by extrapolation, by inference from seismic observations, from knowledge of the behaviour of materials at high temperatures and pressures, from metamorphic rocks and from models of the distribution of heat production and of the Earth's thermal evolution.

7.2 Conductive heat flow

7.2.1 The heat-conduction equation

Heat, as everyone knows, flows from a hot body to a cold body, not the other way around. The *rate* at which heat is conducted through a solid is proportional to the temperature gradient (the difference in temperature per unit length). Heat is conducted faster when there is a large temperature gradient than when there is a small temperature gradient (all other things remaining constant). Imagine an infinitely long and wide solid plate, d in thickness, with its upper surface kept at temperature T_1 and its lower surface at temperature T_2 ($T_2 > T_1$). The rate of flow of heat per unit area *up* through the plate is proportional to

$$\frac{T_2 - T_1}{d} \quad (7.1)$$

The rate of flow of heat per unit area *down* through the plate, Q , is therefore

$$Q = -k \frac{T_2 - T_1}{d} \quad (7.2)$$

where k , the constant of proportionality, is called the *thermal conductivity*. The thermal conductivity is a physical property of the material of which the plate is made and is a measure of its physical ability to conduct heat. The rate of flow of heat per unit area Q is measured in units of watts per square metre (W m^{-2}), and thermal conductivity k is in watts per metre per degree centigrade

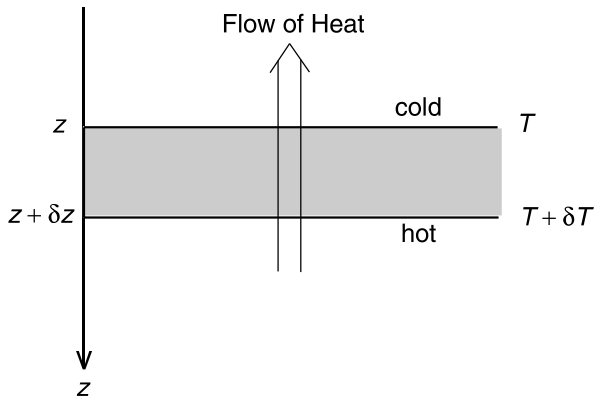


Figure 7.1. Conductive transfer of heat through an infinitely wide and long plate δz in thickness. Heat flows from the hot side of the slab to the cold side (in the negative z direction).

($\text{W m}^{-1} \text{C}^{-1}$).¹ Thermal conductivities of solids vary widely: $418 \text{ W m}^{-1} \text{C}^{-1}$ for silver; $159 \text{ W m}^{-1} \text{C}^{-1}$ for magnesium; $1.2 \text{ W m}^{-1} \text{C}^{-1}$ for glass; $1.7\text{--}3.3 \text{ W m}^{-1} \text{C}^{-1}$ for rock; and $0.1 \text{ W m}^{-1} \text{C}^{-1}$ for wood.

To express Eq. (7.2) as a differential equation, let us assume that the temperature of the upper surface (at z) is T and that the temperature of the lower surface (at $z + \delta z$) is $T + \delta T$ (Fig. 7.1). Substituting these values into Eq. (7.2) then gives

$$Q(z) = -k \frac{T + \delta T - T}{\delta z} \quad (7.3)$$

In the limit as $\delta z \rightarrow 0$, Eq. (7.3) is written

$$Q(z) = -k \frac{\partial T}{\partial z} \quad (7.4)$$

The minus sign in Eq. (7.4) arises because the temperature is increasing in the positive z direction (i.e., downwards); since heat flows from a hot region to a cold region, it flows in the negative z direction (i.e., upwards).

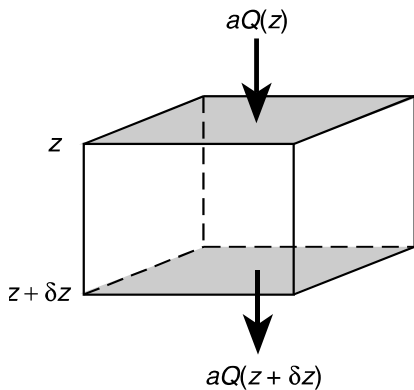
If we consider Eq. (7.4) in the context of the Earth, z denotes depth beneath the surface. Since z increases downwards, a positive temperature gradient (temperature increases with depth) means that there is a net flow of heat upwards out of the Earth. Measurement of temperature gradients and thermal conductivity in near-surface boreholes and mines can provide estimates of the rate of loss of heat from the Earth.

Consider a small volume of height δz and cross-sectional area a (Fig. 7.2). Any change in temperature δT of this small volume in time δt depends on

1. the flow of heat across the volume's surface (net flow is in or out),
2. the heat generated in the volume and
3. the thermal capacity (specific heat) of the material.

¹ Until fairly recently, the c.g.s. system was used in heat-flow work. In that system, 1 hgu (heat-generation unit) = $10^{-13} \text{ cal cm}^{-3} \text{s}^{-1} = 4.2 \times 10^{-7} \text{ W m}^{-3}$; 1 hfu (heat-flow unit) = $10^{-6} \text{ cal cm}^{-2} \text{s}^{-1} = 4.2 \times 10^{-2} \text{ W m}^{-2}$; and thermal conductivity, $0.006 \text{ cal cm}^{-1} \text{s}^{-1} \text{C}^{-1} = 2.52 \text{ W m}^{-1} \text{C}^{-1}$.

Figure 7.2. A volume element of height δz and cross-sectional area a . Heat is conducted into and out of the element across the shaded faces only. We assume that there is no heat transfer across the other four faces.



The heat per unit time entering the volume across its face at z is $aQ(z)$, whereas the heat per unit time leaving the element across its face at $z + \delta z$ is $aQ(z + \delta z)$. Expanding $Q(z + \delta z)$ in a Taylor series gives

$$Q(z + \delta z) = Q(z) + \delta z \frac{\partial Q}{\partial z} + \frac{(\delta z)^2}{2} \frac{\partial^2 Q}{\partial z^2} + \dots \quad (7.5)$$

In the Taylor series, the $(\delta z)^2$ term and those of higher order are very small and can be ignored. From Eq. (7.5) the net gain of heat per unit time is

$$\begin{aligned} & \text{heat entering across } z - \text{heat leaving across } z + \delta z \\ &= aQ(z) - aQ(z + \delta z) \\ &= -a \delta z \frac{\partial Q}{\partial z} \end{aligned} \quad (7.6)$$

Suppose that heat is generated in this volume element at a rate A per unit volume per unit time. The total amount of heat generated per unit time is then

$$Aa \delta z \quad (7.7)$$

Radioactive heat is the main internal heat source for the Earth as a whole; however, local heat sources and sinks include radioactive heat generation (Section 7.2.2), latent heat, shear heating and endothermic and exothermic chemical reactions. Combining expressions (7.6) and (7.7) gives the total gain in heat per unit time to first order in δz as

$$Aa \delta z - a \delta z \frac{\partial Q}{\partial z} \quad (7.8)$$

The *specific heat* c_P of the material of which the volume is made determines the rise in temperature due to this gain in heat since specific heat is defined as *the amount of heat necessary to raise the temperature of 1 kg of the material by 1 °C*. Specific heat is measured in units of $\text{W kg}^{-1} \text{°C}^{-1}$.

If the material has density ρ and specific heat c_P , and undergoes a temperature increase δT in time δt , the rate at which heat is gained is

$$c_P a \delta z \rho \frac{\delta T}{\delta t} \quad (7.9)$$

Thus equating the expressions (7.8) and (7.9) for the rate at which heat is gained by the volume element gives

$$\begin{aligned} c_P a \delta z \rho \frac{\delta T}{\delta t} &= A a \delta z - a \delta z \frac{\partial Q}{\partial z} \\ c_P \rho \frac{\delta T}{\delta t} &= A - \frac{\partial Q}{\partial z} \end{aligned} \quad (7.10)$$

In the limiting case when $\delta z, \delta t \rightarrow 0$, Eq. (7.10) becomes

$$c_P \rho \frac{\partial T}{\partial t} = A - \frac{\partial Q}{\partial z} \quad (7.11)$$

Using Eq. (7.4) for Q (heat flow per unit area), we can write

$$c_P \rho \frac{\partial T}{\partial t} = A + k \frac{\partial^2 T}{\partial z^2} \quad (7.12)$$

or

$$\frac{\partial T}{\partial t} = \frac{k}{\rho c_P} \frac{\partial^2 T}{\partial z^2} + \frac{A}{\rho c_P} \quad (7.13)$$

This is the one-dimensional heat-conduction equation.

In the derivation of this equation, temperature was assumed to be a function solely of time t and depth z . It was assumed not to vary in the x and y directions. If temperature were assumed to be a function of x, y, z and t , a three-dimensional heat-conduction equation could be derived in the same way as this one-dimensional equation. It is not necessary to go through the algebra again: we can generalize Eq. (7.13) to a three-dimensional Cartesian coordinate system as

$$\frac{\partial T}{\partial t} = \frac{k}{\rho c_P} \left(\frac{\partial^2 T}{\partial x^2} + \frac{\partial^2 T}{\partial y^2} + \frac{\partial^2 T}{\partial z^2} \right) + \frac{A}{\rho c_P} \quad (7.14)$$

Using differential-operator notation (see Appendix 1), we write Eq. (7.14) as

$$\frac{\partial T}{\partial t} = \frac{k}{\rho c_P} \nabla^2 T + \frac{A}{\rho c_P} \quad (7.15)$$

Equations (7.14) and (7.15) are known as the *heat-conduction equation*. The term $k/(\rho c_P)$ is known as the *thermal diffusivity* κ . Thermal diffusivity expresses the ability of a material to lose heat by conduction. Although we have derived this equation for a Cartesian coordinate system, we can use it in any other coordinate system (e.g., cylindrical or spherical), provided that we remember to use the definition of the Laplacian operator, ∇^2 (Appendix 1), which is appropriate for the desired coordinate system.

For a steady-state situation when there is no change in temperature with time, Eq. (7.15) becomes

$$\nabla^2 T = -\frac{A}{k} \quad (7.16)$$

In the special situation when there is no heat generation, Eq. (7.15) becomes

$$\frac{\partial T}{\partial t} = \frac{k}{\rho c_P} \nabla^2 T \quad (7.17)$$

This is the *diffusion equation* (Section 7.3.5).

So far we have assumed that there is no relative motion between the small volume of material and its immediate surroundings. Now consider how the temperature of the small volume changes with time if it is in relative motion through a region where the temperature varies with depth. This is an effect not previously considered, so Eq. (7.13) and its three-dimensional analogue, Eq. (7.15), must be modified. Assume that the volume element is moving with velocity u_z in the z direction. It is now no longer fixed at depth z ; instead, at any time t , its depth is $z + u_z t$. The $\partial T / \partial t$ in Eq. (7.13) must therefore be replaced by

$$\frac{\partial T}{\partial t} + \frac{dz}{dt} \frac{\partial T}{\partial z}$$

The first term is the variation of temperature with time at a fixed depth z in the region. The second term

$$\frac{dz}{dt} \frac{\partial T}{\partial z}$$

is equal to $u_z \partial T / \partial z$ and accounts for the effect of the motion of the small volume of material through the region where the temperature varies with depth. Equations (7.13) and (7.15) become, respectively,

$$\frac{\partial T}{\partial t} = \frac{k}{\rho c_P} \frac{\partial^2 T}{\partial z^2} + \frac{A}{\rho c_P} - u_z \frac{\partial T}{\partial z} \quad (7.18)$$

and

$$\frac{\partial T}{\partial t} = \frac{k}{\rho c_P} \nabla^2 T + \frac{A}{\rho c_P} - \mathbf{u} \cdot \nabla T \quad (7.19)$$

In Eq. (7.19), \mathbf{u} is the three-dimensional velocity of the material. The term $\mathbf{u} \cdot \nabla T$ is the *advection-transfer* term.

Relative motion between the small volume and its surroundings can occur for various reasons. The difficulty involved in solving Eqs. (7.18) and (7.19) depends on the cause of this relative motion. If material is being eroded from above the small volume or deposited on top of it, then the volume is becoming nearer to or further from the cool surface of the Earth. In these cases, u_z is the rate at which erosion or deposition is taking place. This is the process of advection referred to earlier. On the other hand, the volume element may form part of a thermal-convection cell driven by temperature-induced differences in density. In the latter case, the value of u_z depends on the temperature field itself rather than on an external factor such as erosion rates. The fact that, for convection, u_z is a function of temperature means that Eqs. (7.18) and (7.19) are nonlinear and hence significantly more difficult to solve (Section 8.2.2).

7.2.2 Radioactive heat generation

Heat is produced by the decay of radioactive isotopes (Table 6.2). Those radioactive elements which contribute most to the internal heat generation of the Earth are uranium, thorium and potassium. These elements are present in the crust in

very small quantities, parts per million for uranium and thorium and of the order of 1% for potassium; in the mantle they are some two orders of magnitude less abundant. Nevertheless, these radioactive elements are important in determining the temperature and tectonic history of the Earth. Other radioactive isotopes, such as aluminium-26 and plutonium-244, have been important in the earliest history of the planet.

The radioactive isotopes producing most of the heat generation in the crust are ^{238}U , ^{235}U , ^{232}Th and ^{40}K . The uranium in the crust can be considered to be ^{238}U and ^{235}U , with present-day relative abundances of 99.28% and 0.72%, respectively; but ^{40}K is present at a level of merely one in 10^4 of total potassium (Chapter 6). The radioactive heat generation for these elements in the Earth is therefore as follows: uranium, $9.8 \times 10^{-5} \text{ W kg}^{-1}$; thorium, $2.6 \times 10^{-5} \text{ W kg}^{-1}$; and potassium, $3.5 \times 10^{-9} \text{ W kg}^{-1}$. Table 7.1 gives the radioactive heat generation of some average rock types. It is clear from this table that, on average, the contributions of uranium and thorium to heat production are larger than that of potassium. On average, granite has a greater internal heat generation than do mafic igneous rocks, and the heat generation of undepleted mantle is very low.

The heat generated by these radioactive isotopes when measured today can be used to calculate the heat generated at earlier times. At time t ago, a radioactive isotope with a decay constant λ would have been a factor $e^{\lambda t}$ more abundant than it is today (Eq. (6.5)). Table 7.2 shows the changes in abundance of isotopes and consequent higher heat generation in the past relative to the present.

Although the heat generation of the crust is some two orders of magnitude greater than that of the mantle, the rate at which the Earth as a whole produces heat is influenced by the mantle because the volume of the mantle is so much greater than the total crustal volume. About one-fifth of radioactive heat is generated in the crust. The mean abundances of potassium, thorium and uranium, for the crust and mantle taken together, are in the ranges 150–260 ppm, 80–100 ppb and 15–25 ppb, respectively. These abundances result in a total radioactive heat production for the crust and mantle of $(1.4\text{--}2.7) \times 10^{13} \text{ W}$, with a best-guess value of $2.1 \times 10^{13} \text{ W}$.

7.3 Calculation of simple geotherms

7.3.1 Equilibrium geotherms

As can be seen from Eq. (7.18), the temperature in a column of rock is controlled by several parameters, some internal and some external to the rock column. The internal parameters are the conductivity, specific heat, density and radioactive heat generation. External factors include heat flow into the column, the surface temperature and the rate at which material is removed from or added to the top of the column (erosion or deposition). Temperature-depth profiles within the Earth are called *geotherms*. If we consider a one-dimensional column with no erosion

Table 7.1 *Typical concentrations of radioactive elements and heat production of some rock types*

	Granite	Tholeiitic basalt	Alkali basalt	Peridotite	Average continental upper crust	Average continental crust	Average oceanic crust	Undepleted mantle
Concentration by weight								
U (ppm)	4	0.1	0.8	0.006	2.8	1.1	0.9	0.02
Th (ppm)	15	0.4	2.5	0.04	10.7	4.2	2.7	0.10
K (%)	3.5	0.2	1.2	0.01	3.4	1.3	0.4	0.04
Heat generation ($10^{-10} \text{ W kg}^{-1}$)								
U	3.9	0.1	0.8	0.006	2.8	1.1	0.9	0.02
Th	4.1	0.1	0.7	0.010	3.0	1.2	0.7	0.03
K	1.3	0.1	0.4	0.004	1.2	0.5	0.1	0.007
Total	9.3	0.3	1.9	0.020	7.0	2.7	1.7	0.057
Density (10^3 kg m^{-3})	2.7	2.8	2.7	3.2	2.7	2.7	2.9	3.2
Heat generation ($\mu\text{W m}^{-3}$)	2.5	0.08	0.5	0.006	1.8	0.7	0.5	0.02

Table 7.2 *Relative abundances of isotopes and crustal heat generation in the past relative to the present*

Age (Ma)	Relative abundance					Heat generation	
	^{238}U	^{235}U	U^{a}	Th	K	Model A ^b	Model B ^c
Present	1.00	1.00	1.00	1.00	1.00	1.00	1.00
500	1.08	1.62	1.10	1.03	1.31	1.13	1.17
1000	1.17	2.64	1.23	1.05	1.70	1.28	1.37
1500	1.26	4.30	1.39	1.08	2.22	1.48	1.64
2000	1.36	6.99	1.59	1.10	2.91	1.74	1.98
2500	1.47	11.4	1.88	1.13	3.79	2.08	2.43
3000	1.59	18.5	2.29	1.16	4.90	2.52	3.01
3500	1.71	29.9	2.88	1.19	6.42	3.13	3.81

^a This assumes a present-day isotopic composition of 99.2886% ^{238}U and 0.7114% ^{235}U .

^b Model A, based on $\text{Th}/\text{U} = 4$ and $\text{K}/\text{U} = 20\,000$.

^c Model B, based on $\text{Th}/\text{U} = 4$ and $\text{K}/\text{U} = 40\,000$.

Source: Jessop and Lewis (1978).

or deposition and a constant heat flow, the column may eventually reach a state of thermal equilibrium in which the temperature at any point is steady. In that case, the temperature–depth profile is called an *equilibrium geotherm*. In this equilibrium situation, $\partial T/\partial t = 0$ and Eq. (7.16) applies:

$$\frac{\partial^2 T}{\partial z^2} = -\frac{A}{k} \quad (7.20)$$

Since this is a second-order differential equation, it can be solved given two boundary conditions. Assume that the surface is at $z = 0$ and that z increases downwards. Let us consider two pairs of boundary conditions. One possible pair is

- (i) temperature $T = 0$ at $z = 0$ and
- (ii) surface heat flow $Q = -k \partial T/\partial z = -Q_0$ at $z = 0$.

The surface heat flow $Q = -Q_0$ is negative because heat is assumed to be flowing upwards out of the medium, which is in the negative z direction. Integrating Eq. (7.20) once gives

$$\frac{\partial T}{\partial z} = -\frac{Az}{k} + c_1 \quad (7.21)$$

where c_1 is the constant of integration. Because $\partial T/\partial z = Q_0/k$ at $z = 0$ is boundary condition (ii), the constant c_1 is given by

$$c_1 = \frac{Q_0}{k} \quad (7.22)$$

Substituting Eq. (7.22) into Eq. (7.21) and then integrating the second time gives

$$T = -\frac{A}{2k}z^2 + \frac{Q_0}{k}z + c_2 \quad (7.23)$$

where c_2 is the constant of integration. However, since $T = 0$ at $z = 0$ was specified as boundary condition (i), c_2 must equal zero. The temperature within the column is therefore given by

$$T = -\frac{A}{2k}z^2 + \frac{Q_0}{k}z \quad (7.24)$$

An alternative pair of boundary conditions could be

- (i) temperature $T = 0$ at $z = 0$ and
- (ii) heat flow $Q = -Q_d$ at $z = d$.

This could, for example, be used to estimate equilibrium crustal geotherms if d was the depth of the crust/mantle boundary and Q_d was the mantle heat flow into the base of the crust. For these boundary conditions, integrating Eq. (7.20) gives, as before,

$$\frac{\partial T}{\partial z} = -\frac{A}{k}z + c_1 \quad (7.25)$$

where c_1 is the constant of integration. Because $\partial T / \partial z = Q_d / k$ at $z = d$ is boundary condition (ii), c_1 is given by

$$c_1 = \frac{Q_d}{k} + \frac{Ad}{k} \quad (7.26)$$

Substituting Eq. (7.26) into Eq. (7.25) and then integrating again gives

$$T = -\frac{A}{2k}z^2 + \frac{Q_d + Ad}{k}z + c_2 \quad (7.27)$$

where c_2 is the constant of integration. Because $T = 0$ at $z = 0$ was boundary condition (i), c_2 must equal zero. The temperature in the column $0 \leq z \leq d$ is therefore given by

$$T = -\frac{A}{2k}z^2 + \frac{Q_d + Ad}{k}z \quad (7.28)$$

Comparison of the second term in Eq. (7.24) with that in Eq. (7.28) shows that a column of material of thickness d and radioactive heat generation A makes a contribution to the surface heat flow of Ad . Similarly, the mantle heat flow Q_d contributes $Q_d z / k$ to the temperature at depth z .

7.3.2 One-layer models

Figure 7.3 illustrates how the equilibrium geotherm for a model rock column changes when the conductivity, radioactive heat generation and basal heat flow

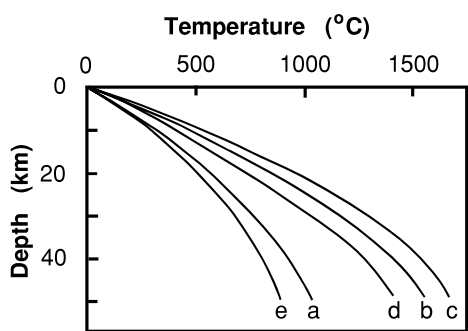


Figure 7.3. Equilibrium geotherms calculated from Eq. (7.28) for a 50-km-thick column of rock. Curve a: standard model with conductivity $2.5 \text{ W m}^{-1} \text{ }^{\circ}\text{C}^{-1}$, radioactive heat generation $1.25 \mu\text{W m}^{-3}$ and basal heat flow $21 \times 10^{-3} \text{ W m}^{-2}$. Curve b: standard model with conductivity reduced to $1.7 \text{ W m}^{-1} \text{ }^{\circ}\text{C}^{-1}$. Curve c: standard model with radioactive heat generation increased to $2.5 \mu\text{W m}^{-3}$. Curve d: standard model with basal heat flow increased to $42 \times 10^{-3} \text{ W m}^{-2}$. Curve e: standard model with basal heat flow reduced to $10.5 \times 10^{-3} \text{ W m}^{-2}$. (From Nisbet and Fowler (1982).)

are varied. This model column is 50 km thick, has conductivity $2.5 \text{ W m}^{-1} \text{ }^{\circ}\text{C}^{-1}$, radioactive heat generation $1.25 \mu\text{W m}^{-3}$ and a heat flow into the base of the column of $21 \times 10^{-3} \text{ W m}^{-2}$. The equilibrium geotherm for this model column is given by Eq. (7.28) and is shown as curve a in Fig. 7.3; at shallow levels the gradient is approximately $30 \text{ }^{\circ}\text{C km}^{-1}$, whereas at deep levels the gradient is $15 \text{ }^{\circ}\text{C km}^{-1}$ or less.

Conductivity

Reducing the conductivity of the whole column to $1.7 \text{ W m}^{-1} \text{ }^{\circ}\text{C}^{-1}$ has the effect of increasing the shallow-level gradient to about $45 \text{ }^{\circ}\text{C km}^{-1}$ (see curve b in Fig. 7.3). Increasing the conductivity to $3.4 \text{ W m}^{-1} \text{ }^{\circ}\text{C}^{-1}$ would have the opposite effect of reducing the gradient to about $23 \text{ }^{\circ}\text{C km}^{-1}$ at shallow levels.

Heat generation

Increasing the heat generation from $1.25 \mu\text{W m}^{-3}$ to $2.5 \mu\text{W m}^{-3}$ raises the shallow-level gradient to over $50 \text{ }^{\circ}\text{C km}^{-1}$ (curve c in Fig. 7.3); in contrast, reducing the heat generation to $0.4 \mu\text{W m}^{-3}$ reduces this shallow-level gradient to about $16 \text{ }^{\circ}\text{C km}^{-1}$.

Basal heat flow

If the basal heat flow is doubled from 21×10^{-3} to $42 \times 10^{-3} \text{ W m}^{-2}$, the gradient at shallow level is increased to about $40 \text{ }^{\circ}\text{C km}^{-1}$ (curve d in Fig. 7.3). If the basal heat flow is halved to $10.5 \times 10^{-3} \text{ W m}^{-2}$, the shallow-level gradient is reduced to about $27 \text{ }^{\circ}\text{C km}^{-1}$ (curve e in Fig. 7.3).

7.3.3 Two-layer models

The models described so far have been very simple, with a 50-km-thick surface layer of uniform composition. This is not appropriate for the real Earth but is a mathematically simple illustration. More realistic models have a layered crust with the heat generation concentrated towards the top (see, e.g., Section 7.6.1). The equilibrium geotherm for such models is calculated exactly as described in Eqs. (7.20)–(7.28) except that each layer must be considered separately and temperature and temperature gradients must be matched across the boundaries.

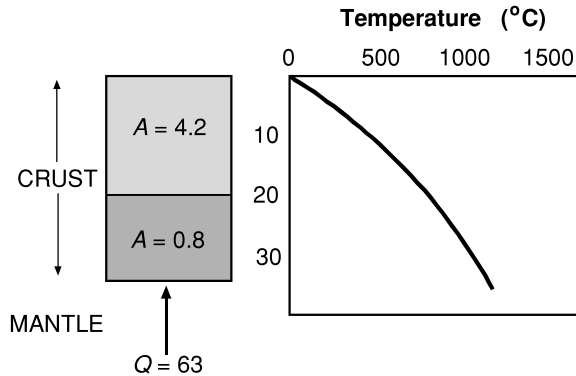


Figure 7.4. A two-layer model for the crust and equilibrium geotherm in the Archaean. Heat generation A is in $\mu\text{W m}^{-3}$; heat flow from the mantle Q is in 10^{-3} W m^{-2} . Recall that, during the Archaean, heat generation was much greater than it is now (Table 7.2). (After Nisbet and Fowler (1982).)

Consider a two-layer model:

$$A = A_1 \quad \text{for } 0 \leq z < z_1$$

$$A = A_2 \quad \text{for } z_1 \leq z < z_2$$

$$T = 0 \quad \text{on } z = 0$$

with a basal heat flow $Q = -Q_2$ on $z = z_2$. In the first layer, $0 \leq z < z_1$, the equilibrium heat-conduction equation is

$$\frac{\partial^2 T}{\partial z^2} = -\frac{A_1}{k} \quad (7.29)$$

In the second layer, $z_1 \leq z < z_2$, the equilibrium heat-conduction equation is

$$\frac{\partial^2 T}{\partial z^2} = -\frac{A_2}{k} \quad (7.30)$$

The solution to these two differential equations, subject to the boundary conditions and matching both temperature, T , and temperature gradient, $\partial T / \partial z$, on the boundary $z = z_1$, is

$$T = -\frac{A_1}{2k}z^2 + \left(\frac{Q_2}{k} + \frac{A_2}{k}(z_2 - z_1) + \frac{A_1 z_1}{k} \right)z \quad \text{for } 0 \leq z < z_1 \quad (7.31)$$

$$T = -\frac{A_2}{2k}z^2 + \left(\frac{Q_2}{k} + \frac{A_2 z_2}{k} \right)z + \frac{A_1 - A_2}{2k}z_1^2 \quad \text{for } z_1 \leq z < z_2 \quad (7.32)$$

Figure 7.4 shows an equilibrium geotherm calculated for a model Archaean crust. The implication is that, during the Archaean, crustal temperatures may have been relatively high (compare with Fig. 7.3.).

7.3.4 The timescale of conductive heat flow

Geological structures such as young mountain belts are not usually in thermal equilibrium because the thermal conductivity of rock is so low that it takes many millions of years to attain equilibrium. For example, consider the model rock column with the geotherm shown as curve a in Fig. 7.3. If the basal heat flow were suddenly increased from 21×10^{-3} to $42 \times 10^{-3} \mu\text{W m}^{-2}$, the temperature of the column would increase until the new equilibrium temperatures were attained (curve d in Fig. 7.3). That this process is very slow can be illustrated by considering a rock at depth 20 km. The initial temperature at 20 km would be 567°C , and, 20 Ma after the basal heat flow increased, conduction would have raised the temperature at 20 km to about 580°C . Only after 100 Ma would the temperature at 20 km be over 700°C and close to the new equilibrium value of 734°C . This can be estimated quantitatively from Eq. (7.17):

$$\frac{\partial T}{\partial t} = \kappa \frac{\partial^2 T}{\partial z^2}$$

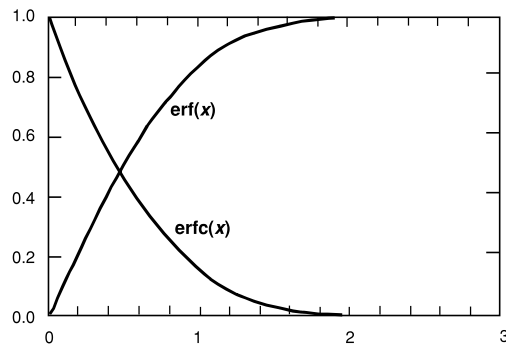
The *characteristic time* $\tau = l^2/\kappa$ gives an indication of the amount of time necessary for a change in temperature to propagate a distance of l in a medium having thermal diffusivity κ . Likewise, the *characteristic thermal diffusion distance*, $l = \sqrt{\kappa\tau}$, gives an indication of the distance that changes in temperature propagate during a time τ . To give a geological example, it would take many tens of millions of years for thermal transfer from a subduction zone at 100 km depth to have a significant effect on the temperatures at shallow depth if all heat transfer were by conduction alone. Hence, melting and intrusion are important mechanisms for heat transfer above subduction zones. As a second example, a metamorphic belt caused by a deep-seated heat source is characterized by abundant intrusions, often of mantle-derived material; this is the dominant factor in transfer of heat to the surface. Magmatism occurs because large increases in the deep heat flow cause large-scale melting at depth long before the heat can penetrate very far towards the surface by conduction.

When a rock column is assembled by some process such as sedimentation, overthrusting or intrusion, the initial temperature gradient is likely to be very different from the equilibrium gradient. This should always be borne in mind when evaluating thermal problems.

7.3.5 Instantaneous cooling or heating

Assume that there is a semi-infinite solid with an upper surface at $z = 0$, no heat generation ($A = 0$) and an initial temperature throughout the solid of $T = T_0$. For $t > 0$, let the surface be kept at temperature $T = 0$. We want to determine how the interior of the solid cools with time.

Figure 7.5. The error function $\text{erf}(x)$ and complementary error function $\text{erfc}(x)$.



The differential equation to be solved is Eq. (7.13) with $A = 0$, the *diffusion equation*:

$$\frac{\partial T}{\partial t} = \kappa \frac{\partial^2 T}{\partial z^2} \quad (7.33)$$

where $\kappa = k / (\rho c_P)$ is the thermal diffusivity.

Derivation of the solution to this problem is beyond the scope of this book, and the interested reader is referred to Carslaw and Jaeger (1959), Chapter 2, or Turcotte and Schubert (2002), Chapter 4. Here we merely state that the solution of this equation which satisfies the boundary conditions is given by an *error function* (Fig. 7.5 and Appendix 5):

$$T = T_0 \text{erf}\left(\frac{z}{2\sqrt{\kappa t}}\right) \quad (7.34)$$

The error function is defined by

$$\text{erf}(x) = \frac{2}{\sqrt{\pi}} \int_0^x e^{-y^2} dy \quad (7.35)$$

You can check that Eq. (7.34) is a solution to Eq. (7.33) by differentiating with respect to t and z . Equation (7.34) shows that the time taken to reach a given temperature is proportional to z^2 and inversely proportional to κ .

The temperature gradient is given by differentiating Eq. (7.34) with respect to z :

$$\begin{aligned} \frac{\partial T}{\partial z} &= \frac{\partial}{\partial z} \left[T_0 \text{erf}\left(\frac{z}{2\sqrt{\kappa t}}\right) \right] \\ &= T_0 \frac{2}{\sqrt{\pi}} \frac{1}{2\sqrt{\kappa t}} e^{-z^2/(4\kappa t)} \\ &= \frac{T_0}{\sqrt{\pi \kappa t}} e^{-z^2/(4\kappa t)} \end{aligned} \quad (7.36)$$

This error-function solution to the heat-conduction equation can be applied to many geological situations. For solutions to these problems, and numerous others, the reader is again referred to Carslaw and Jaeger (1959).

For example, imagine a dyke of width $2w$ and of infinite extent in the y and z directions. If we assume that there is no heat generation and that the dyke has an initial temperature of T_0 , and if we ignore latent heat of solidification, then the differential equation to be solved is

$$\frac{\partial T}{\partial t} = \kappa \frac{\partial^2 T}{\partial z^2}$$

with initial conditions

- (i) $T = T_0$ at $t = 0$ for $-w \leq x \leq w$ and
- (ii) $T = 0$ at $t = 0$ for $|x| > w$.

The solution of this equation which satisfies the initial conditions is

$$T(x, t) = \frac{T_0}{2} \left[\operatorname{erf} \left(\frac{w-x}{2\sqrt{\kappa t}} \right) + \operatorname{erf} \left(\frac{w+x}{2\sqrt{\kappa t}} \right) \right] \quad (7.37)$$

If the dyke were 2 m in width ($w = 1$ m) and intruded at a temperature of 1000 °C and if κ were 10^{-6} m² s⁻¹, then the temperature at the centre of the dyke would be about 640 °C after one week, 340 °C after one month and only about 100 °C after one year! Clearly, a small dyke cools very rapidly.

For the general case, the temperature in the dyke is about $T_0/2$ when $t = w^2/\kappa$ and about $T_0/4$ when $t = 5w^2/\kappa$. High temperatures outside the dyke are confined to a narrow contact zone: at a distance w away from the edge of the dyke the highest temperature reached is only about $T_0/4$. Temperatures close to $T_0/2$ are reached only within about $w/4$ of the edge of the dyke.

Example: periodic variation of surface temperature

Because the Earth's surface temperature is not constant but varies periodically (daily, annually, ice ages), it is necessary to ensure that temperature measurements are made deep enough that distortion due to these surface periodicities is minimal. We can model this periodic contribution to the surface temperature as $T_0 e^{i\omega t}$, where ω is 2π multiplied by the frequency of the temperature variation, i is the square root of -1 and T_0 is the maximum variation of the mean surface temperature. The temperature $T(z, t)$ is then given by Eq. (7.13) (with $A = 0$) subject to the following two boundary conditions:

- (i) $T(0, t) = T_0 e^{i\omega t}$ and
- (ii) $T(z, t) \rightarrow 0$ as $z \rightarrow \infty$.

We can use the separation-of-variables technique to solve this problem. Let us assume that the variables z and t can be separated and that the temperature can be written as

$$T(z, t) = V(z)W(t) \quad (7.38)$$

This supposes that the periodic nature of the temperature variation is the same at all depths as it is at the surface, but it allows the magnitude and phase of the variation

to be depth-dependent, which seems reasonable. Substitution into Eq. (7.13) (with $A = 0$) then yields

$$V \frac{dW}{dt} = \frac{k}{\rho c_P} W \frac{d^2 V}{dz^2} \quad (7.39)$$

which, upon rearranging, becomes

$$\frac{1}{W} \frac{dW}{dt} = \frac{k}{\rho c_P} \frac{1}{V} \frac{d^2 V}{dz^2} \quad (7.40)$$

Because the left-hand side of this equation is a function of z alone and the right-hand side is a function of t alone, it follows that each must equal a constant, say, c_1 . However, substitution of Eq. (7.38) into the boundary conditions (i) and (ii) yields, respectively,

$$W(t) = e^{i\omega t} \quad (7.41)$$

and

$$V(z) \rightarrow 0 \quad \text{as } z \rightarrow \infty \quad (7.42)$$

Boundary condition (i) therefore means that the constant c_1 must be equal to $i\omega$ (differentiate Eq. (7.41) to check this). Substituting Eq. (7.41) into Eq. (7.40) gives the equation to be solved for $V(z)$:

$$\frac{d^2 V}{dz^2} = \frac{i\omega \rho c_P V}{k} \quad (7.43)$$

This has the solution

$$V(z) = c_2 e^{-qz} + c_3 e^{qz} \quad (7.44)$$

where $q = (1 + i)\sqrt{\omega \rho c_P / (2k)}$ (remember that $\sqrt{i} = (1 + i)/\sqrt{2}$) and c_2 and c_3 are constants. Equation (7.37), boundary condition (ii), indicates that the positive exponential solution is not allowed; the constant c_3 must be zero. Boundary condition (i) indicates that the constant c_2 is T_0 ; so, finally, $T(z, t)$ is given by

$$\begin{aligned} T(z, t) &= T_0 \exp(i\omega t) \exp\left(-(1 + i)\sqrt{\frac{\omega \rho c_P}{2k}} z\right) \\ &= T_0 \exp\left(-\sqrt{\frac{\omega \rho c_P}{2k}} z\right) \exp\left[i\left(\omega t - \sqrt{\frac{\omega \rho c_P}{2k}} z\right)\right] \end{aligned} \quad (7.45)$$

For large z this periodic variation dies out. Thus, temperatures at great depth are unaffected by the variations in surface temperatures, as required by boundary condition (ii).

At a depth of

$$L = \sqrt{\frac{2k}{\omega \rho c_P}} \quad (7.46)$$

the periodic disturbance has an amplitude $1/e$ of the amplitude at the surface. This depth L is called the skin depth. Taking $k = 2.5 \text{ W m}^{-1} \text{ }^\circ\text{C}^{-1}$, $c_P = 10^3 \text{ J kg}^{-1} \text{ }^\circ\text{C}^{-1}$ and $\rho = 2.3 \times 10^3 \text{ kg m}^{-3}$, which are reasonable values for a sandstone, then for the daily variation ($\omega = 7.27 \times 10^{-5} \text{ s}^{-1}$), L is approximately 17 cm; for the annual

variation ($\omega = 2 \times 10^{-7} \text{ s}^{-1}$), L is 3.3 m; and for an ice age (with period of the order of 100 000 yr), L is greater than 1 km. Therefore, provided that temperature measurements are made at depths greater than 10–20 m, the effects of the daily and annual surface temperature variation are negligible. The effects of ice ages cannot be so easily ignored and must be considered when borehole measurements are made. Measurement of temperatures in ocean sediments is not usually subject to these constraints, the ocean-bottom temperature being comparatively constant.

Equation (7.45) shows that there is a phase difference ϕ between the surface temperature variation and that at depth z ,

$$\phi = \sqrt{\frac{\omega \rho c_p}{2k}} z \quad (7.47)$$

At the skin depth, this phase difference is one radian. When the phase difference is π , the temperature at depth z is exactly half a cycle out of phase with the surface temperature.

7.4 Worldwide heat flow: total heat loss from the Earth

The total present-day worldwide rate of heat loss by the Earth is estimated to be $(4.2\text{--}4.4) \times 10^{13} \text{ W}$. Table 7.3 shows how this heat loss is distributed by area: 71% of this heat loss occurs through the oceans (which cover 60% of the Earth's surface). Thus, most of the heat loss results from the creation and cooling of oceanic lithosphere as it moves away from the mid-ocean ridges. Plate tectonics is a primary consequence of a cooling Earth. Conversely, it seems clear that the mean rate of plate generation is determined by some balance between the total rate at which heat is generated within the Earth and the rate of heat loss at the surface. Some models of the thermal behaviour of the Earth during the Archaean (before 2500 Ma) suggest that the plates were moving around the surface of the Earth an order of magnitude faster than they are today. Other models suggest less marked differences from the present. The heat generated within the Archaean Earth by long-lived radioactive isotopes was probably three-to-four times greater than that generated now (see Table 7.2). A large amount of heat also has been left over from the gravitational energy that was dissipated during accretion of the Earth (see Problem 23) and from short-lived but energetic isotopes such as ^{26}Al , which decayed during the first few million years of the Earth's history.

Evidence from Archaean lavas that were derived from the mantle suggests that the Earth has probably cooled by several hundred degrees since the Archaean as the original inventory of heat has dissipated. The Earth is gradually cooling, and the plates and rates of plate generation may be slowing to match. Presumably, after many billion years all plate motion will cease.

Measured values of heat flow depend on the age of the underlying crust, be it oceanic or continental (Figs. 7.6 and 7.11). Over the oceanic crust the heat flow generally decreases with age: the highest and very variable measurements occur

Table 7.3 Heat loss and heat flow from the Earth

	Area (10^6 km^2)	Mean heat flow (10^3 W m^{-2})	Heat loss (10^{12} W)
Continents (post-Archaean)	142	63	9.0
Archaean	13	52	0.7
Continental shelves	46	78	3.5
Total continental area	201	65 ± 1.6	13.1 ± 0.3
Oceans (including marginal basins)	309	101 ± 2.2	31.2 ± 0.7
Worldwide total	510	87 ± 2.0	44.2 ± 1.0

Note: The estimate of convective heat transport by plates is $\sim 65\%$ of the total heat loss; this includes lithospheric creation in oceans and magmatic activity on continents. The estimate of heat loss as a result of radioactive decay in the crust is $\sim 17\%$ of the total heat loss. Although oceanic regions younger than 66 Ma amount to one-third of the Earth's surface area, they account for over half the total global heat loss. About one-third of the heat loss in oceanic regions is by hydrothermal flow. The estimate of the heat loss of the core is $10^{12}\text{--}10^{13} \text{ W}$; this is a major heat source for the mantle.

Source: Pollack *et al.* (1993).

over the mid-ocean ridges and young crust, and the lowest values are found over the deep ocean basins. In continental regions the highest heat flows are measured in regions that are subject to the most recent tectonic activity, and the lowest values occur over the oldest, most stable regions of the Precambrian Shield. These oceanic and continental heat-flow observations and their implications are discussed in Sections 7.5 and 7.6.

To apply the heat-conduction equation (7.15) to the Earth as a whole, we need to use spherical polar coordinates (r, θ, ϕ) (refer to Appendix 1). If temperature is not a function of θ or ϕ but only of radius r , Eq. (7.15) is

$$\frac{\partial T}{\partial r} = \frac{k}{\rho c_P} \frac{1}{r^2} \frac{\partial}{\partial r} \left(r^2 \frac{\partial T}{\partial r} \right) + \frac{A}{\rho c_P} \quad (7.48)$$

First let us assume that there is no internal heat generation. The equilibrium temperature is then the solution to

$$\frac{1}{r^2} \frac{\partial}{\partial r} \left(r^2 \frac{\partial T}{\partial r} \right) = 0 \quad (7.49)$$

On integrating once, we obtain

$$r^2 \frac{\partial T}{\partial r} = c_1 \quad (7.50)$$

and integrating the second time gives

$$T = -\frac{c_1}{r} + c_2 \quad (7.51)$$

where c_1 and c_2 are the constants of integration.

Now impose the boundary conditions for a *hollow sphere* $b < r < a$:

- (i) zero temperature $T = 0$ at the surface $r = a$ and
- (ii) constant heat flow $Q = -k\partial T/\partial r = Q_b$ at $r = b$.

The temperature in the spherical shell $b < r < a$ is then given by

$$T = -\frac{Q_b b^2}{k} \left(\frac{1}{a} - \frac{1}{r} \right) \quad (7.52)$$

An expression such as this could be used to estimate a steady temperature for the lithosphere. However, since the thickness of the lithosphere is very small compared with the radius of the Earth, $(a - b)/a \ll 1$, this solution is the same as the solution to the one-dimensional equation (7.28) with $A = 0$.

There is no non-zero solution to Eq. (7.49) for the whole sphere, which has a finite temperature at the origin ($r = 0$). However, there is a steady-state solution to Eq. (7.48) with constant internal heat generation A within the sphere:

$$\begin{aligned} 0 &= \frac{k}{r^2} \frac{\partial}{\partial r} \left(r^2 \frac{\partial T}{\partial r} \right) + A \\ \frac{\partial}{\partial r} \left(r^2 \frac{\partial T}{\partial r} \right) &= -\frac{Ar^2}{k} \end{aligned} \quad (7.53)$$

On integrating twice, the temperature is given by

$$T = -\frac{Ar^2}{6k} - \frac{c_1}{r} + c_2 \quad (7.54)$$

where c_1 and c_2 are the constants of integration.

Let us impose the following two boundary conditions:

- (i) T finite at $r = 0$ and
- (ii) $T = 0$ at $r = a$.

Then Eq. (7.54) becomes

$$T = \frac{A}{6k}(a^2 - r^2) \quad (7.55)$$

and the heat flux is given by

$$-k \frac{dT}{dr} = \frac{Ar}{3} \quad (7.56)$$

The surface heat flow (at $r = a$) is therefore equal to $Aa/3$.

If we model the Earth as a solid sphere with constant thermal properties and uniform heat generation, Eqs. (7.55) and (7.56) yield the temperature at the centre of this model Earth, given a value for the surface heat flow. Assuming values of surface heat flow $80 \times 10^{-3} \text{ W m}^{-2}$, $a = 6370 \text{ km}$ and $k = 4 \text{ W m}^{-1} \text{ }^\circ\text{C}^{-1}$, we obtain a temperature at the centre of this model solid Earth of

$$\begin{aligned} T &= \frac{80 \times 10^{-3} \times 6370 \times 10^3}{2 \times 4} \\ &= 63\,700 \text{ }^\circ\text{C} \end{aligned}$$

This temperature is clearly too high for the real Earth because the temperature at the visible surface of the Sun is only about 5700 °C – the Earth is not a star. The model is unrealistic since, in fact, heat is not conducted but convected through the mantle, and the heat-generating elements are concentrated in the upper crust rather than being uniformly distributed throughout the Earth. These facts mean that the actual temperature at the centre of the Earth is much lower than this estimate. Convection is important because it allows the surface heat flow to exploit the entire internal heat of the Earth, instead of just the surface portions of a conductive Earth (see Section 6.1 for Kelvin's conduction calculation of the age of the Earth).

Another fact that we have neglected to consider is the decrease of the radioactive heat generation with time. Equation (7.48) can be solved for an exponential time decay and a non-uniform distribution of the internal heat generation; the temperature solutions are rather complicated (see Carslaw and Jaeger (1959), Section 9.8, for some examples) and still are not applicable to the Earth because heat is convected through mantle and outer core rather than conducted.

It is thought that the actual temperature at the centre of the Earth is about 7000 °C, on the basis of available evidence: thermal and seismic data, laboratory behaviour of solids at high temperatures and pressures and laboratory melting of iron-rich systems at high pressures.

7.5 Oceanic heat flow

7.5.1 Heat flow and the depth of the oceans

Figure 7.6 shows the mean heat flow as a function of age for the three major oceans. The average heat flow is higher over young oceanic crust but exhibits a much greater standard deviation than does that over the older ocean basins. This decrease of heat flow with increasing age is to be expected if we consider hot volcanic material rising along the axes of the mid-ocean ridges and plates cooling as they move away from the spreading centres. The very scattered heat-flow values measured over young oceanic crust are a consequence of the hydrothermal circulation of sea water through the crust (which is also discussed in Section 9.4.4). Heat flow is locally high in the vicinity of hot-water vents and low where cold sea water enters the crust. Water temperatures approaching 400 °C have been measured at the axes of spreading centres by submersibles, and the presence of hot springs on Iceland (which is located on the Reykjanes Ridge) and other islands or regions proximal to spreading centres is well known. As will be discussed in Chapter 9, the oceanic crust is formed by the intrusion of basaltic magma from below. Contact with sea water causes rapid cooling of the new crust, and many cracks form in the lava flows and dykes. Convection of sea water through the cracked crust occurs, and it is probable that this circulation penetrates through most of the crust, providing an efficient cooling mechanism (unless you drive a Volkswagen, your car's engine is cooled in the same manner). As the newly formed

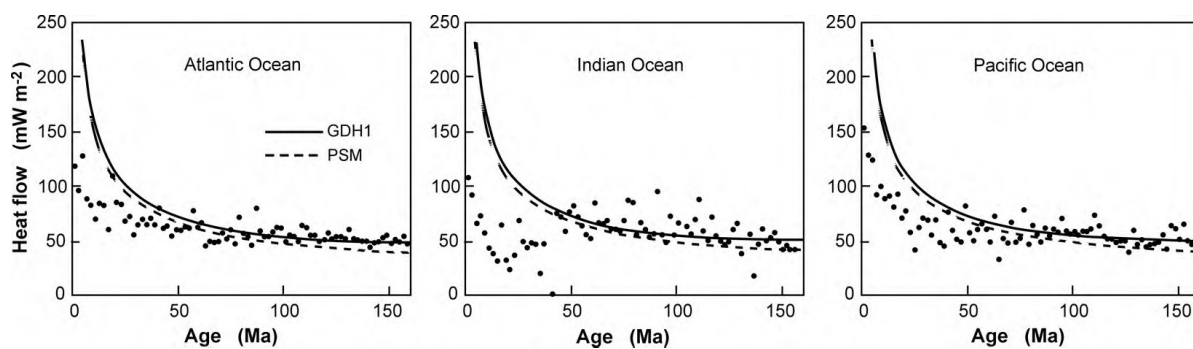


Figure 7.6. Observed heat flows for the Atlantic, Indian and Pacific Oceans. Heat flow predicted by the plate models: solid line, GDH1; and dashed line, PSM. Heat flow predicted by the half-space model HS is not shown – it is almost coincident with PSM (Table 7.5). (After Stein and Stein, Constraints on hydrothermal heat flux through the oceanic lithosphere from global heat data, *J. Geophys. Res.*, **99**, 3881–95, 1994. Copyright 1994 American Geophysical Union. Modified by permission of American Geophysical Union.)

plate moves away from the ridge, sedimentation occurs. Deep-sea sediments have a low permeability² and, in sufficient thickness, are impermeable to sea water. In well-sedimented and therefore generally older crust, measurements of conductive heat flow yield reliable estimates of the actual heat flow. Another important factor affecting cessation of hydrothermal circulation is that, in older crust, pores and cracks will become plugged with mineral deposits. As a result, hydrothermal circulation will largely cease. Loss of heat due to hydrothermal circulation is difficult to measure, so heat-flow estimates for young crust are generally very scattered and also significantly lower than the theoretical estimates of heat loss (Fig. 7.6). That heat-flow measurements are generally less than the predicted values for oceanic lithosphere younger than 65 ± 10 Ma indicates that this is the ‘sealing age’.

As an oceanic plate moves away from the ridge axis and cools, it contracts and thus increases in density. If we assume the oceanic regions to be compensated (see Section 5.5.2), the depth of the oceans should increase with increasing age (and thus plate density). For any model of the cooling lithosphere, the expected ocean depth can be calculated simply (see Section 7.5.2).

Figure 7.7(a) shows the mean depth of the oceans plotted against age. For ages less than 20 Ma a simple relation between bathymetric depth d (km) and lithosphere age t (Ma) is observed:

$$d = 2.6 + 0.365t^{1/2} \quad (7.57a)$$

Depth increases linearly with the square root of age. For ages greater than 20 Ma this simple relation does not hold; depth increases more slowly with increasing

² Permeability and porosity are not the same. Sediments have a higher porosity than that of crustal rocks but lack the connected pore spaces needed for high permeability.

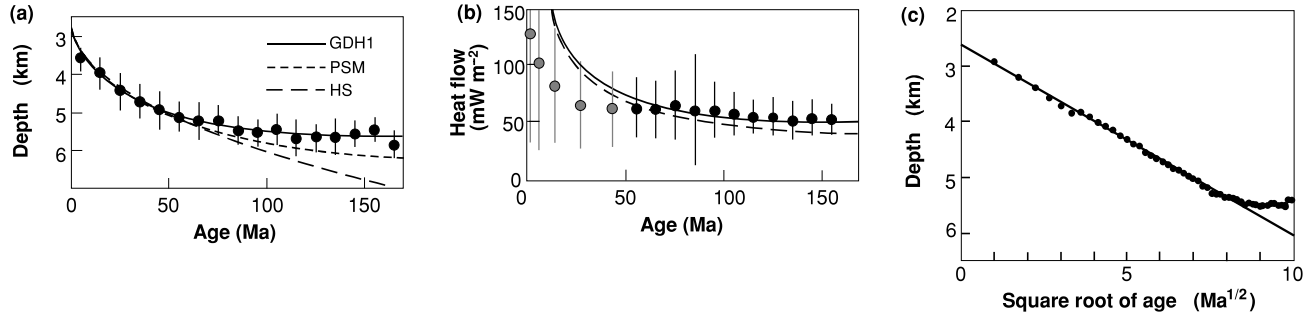


Figure 7.7. Mean oceanic depth (a) and oceanic heat flow (b) with standard deviations plotted every 10 Ma against age. The data are from the north Pacific and northwest Atlantic. These global depths exclude data from the hotspot swells. The three model predictions for ocean depth and heat flow are shown as solid and dashed lines. The plate model GDH1 fits both data sets overall better than does either the half-space model HS or the alternative plate model PSM. Data shown in black were used to determine GDH1. Heat flow data at <50 Ma are shown in grey – these are affected by hydrothermal circulation and were not used to determine GDH1.(c) Mean oceanic depth plotted against the square root of the age of the lithosphere (\sqrt{t}). The solid line is the best-fitting half-space model: $d = 2.607 + 0.344t^{1/2}$. (After Stein and Stein (1992) Thermo-mechanical evolution of oceanic lithosphere: implications for the subduction process and deep earthquakes (overview), Geophysical Monograph 96, 1–17, 1996. Copyright 1996 American Geophysical Union. Modified by Permission of American Geophysical Union; and Carlson and Johnson, On modeling the thermal evolution of the oceanic upper mantle: an assessment of the cooling plate model, *J. Geophys. Res.*, **99**, 3201–14, 1994. Copyright 1994 American Geophysical Union. Modified by permission of American Geophysical Union.)

age and approximates a negative exponential:

$$d = 5.65 - 2.47e^{-t/36} \quad (7.57b)$$

Figure 7.7(b) shows the measured heat flow plotted against age. A simple relationship, linked to that for ocean depth, between heat flow Q (10^{-3} W m⁻²) and lithosphere age t (Ma) is predicted for crust younger than 55 Ma:

$$Q = 510t^{-1/2} \quad (7.58a)$$

Heat flow decreases linearly with the inverse square root of age. For ages greater than 55 Ma this simple relation does not hold; heat flow decreases more slowly with increasing age and follows a negative exponential:

$$Q = 48 + 96e^{-t/36} \quad (7.58b)$$

7.5.2 Models of plate formation and cooling

The creation of a lithospheric plate at the axis of a mid-ocean ridge and the subsequent cooling of the plate as it moves away from the ridge axis give rise to

the type of problem that can be solved by using the two-dimensional version of the heat-conduction equation in a moving medium (Eq. (7.19)). The boundary conditions can be specified in a number of ways: these necessarily lead to different solutions and thus to different estimates of heat flow and bathymetric depth. The bathymetric depth is calculated from the temperature by assuming that the plate is in isostatic equilibrium, and the heat flow is calculated from the temperature gradient at the surface of the lithosphere. In this way, an understanding of the thermal structure and formation of the plates has been built up. As in all scientific work, the best model is the one which best fits the observations, in this case variations of bathymetric depth and heat flow with age.

A simple model

The simplest thermal model of the lithosphere is to assume that the lithosphere is cooled asthenospheric material, which, at the ridge axis, had a constant temperature T_a and no heat generation. If we assume the ridge to be infinite in the y direction and the temperature field to be in equilibrium, then the differential equation to be solved is

$$\frac{k}{\rho c_p} \left(\frac{\partial^2 T}{\partial x^2} + \frac{\partial^2 T}{\partial z^2} \right) = u \frac{\partial T}{\partial x} \quad (7.59)$$

where u is the horizontal velocity of the plate and the term on the right-hand side of the equation is due to advection of heat with the moving plate. A further simplification can be introduced by the assumption that horizontal conduction of heat is insignificant in comparison with horizontal advection and vertical conduction of heat. In this case, we can disregard the $\partial^2 T / \partial x^2$ term, leaving the equation to be solved as

$$\frac{k}{\rho c_p} \frac{\partial^2 T}{\partial z^2} = u \frac{\partial T}{\partial x} \quad (7.60)$$

This equation, however, is identical to Eq. (7.43) if we write $t = x/u$, which means that we reintroduce time through the spreading of the ridge. Approximate initial and boundary conditions are $T = T_a$ at $x = 0$ and $T = 0$ at $z = 0$. According to Eq. (7.44), the solution to Eq. (7.60) is

$$T(z, t) = T_a \operatorname{erf} \left(\frac{z}{2\sqrt{\kappa t}} \right) \quad (7.61)$$

The surface heat flow at any distance (age) from the ridge axis is then obtained by differentiating Eq. (7.61):

$$\begin{aligned} Q(t) &= -k \frac{\partial T}{\partial z} \Big|_{z=0} \\ &= -\frac{k T_a}{\sqrt{\pi \kappa t}} \end{aligned} \quad (7.62)$$

The observed $t^{1/2}$ relationship between heat flow and age is thus a feature of this model which is called a half-space cooling model.

We can estimate the lithospheric thickness L from Eq. (7.61) by specifying a temperature for the base of the lithosphere. For example, if we assume the temperature of the asthenosphere at the ridge axis to be 1300 °C and the temperature at the base of the lithosphere to be 1100 °C, then we need to find the combination of L and t such that

$$1100 = 1300 \operatorname{erf}\left(\frac{L}{2\sqrt{\kappa t}}\right) \quad (7.63)$$

In other words, we need the inverse error function of 0.846. Using Fig. 7.5 (or Appendix 5), we can write

$$1.008 = \frac{L}{2\sqrt{\kappa t}} \quad (7.64)$$

Thus, if $\kappa = 10^{-6} \text{ m}^2 \text{ s}^{-1}$,

$$L = 2.016 \times 10^{-3} \sqrt{t} \quad (7.65a)$$

when L is in metres and t in seconds, or

$$L = 11\sqrt{t} \quad (7.65b)$$

when L is in kilometres and t in millions of years (Ma). At 10 Ma this lithosphere would be 35 km thick, and at 80 Ma it would be 98 km thick. Different choices for the temperature at the ridge axis and at the base of the lithosphere will yield slightly different values for the numerical constants in Eq. (7.65) but the ‘root t ’ dependence of lithosphere thickness on age will not change.

The depth of the seabed at any given age can be calculated by using the principle of isostasy (see Section 5.5.2) and the gradual increase in density of the lithosphere as it cools. If we take the compensation depth D to be in the mantle beneath the base of the lithosphere, the total mass in a vertical column extending down to D is

$$\int_0^D \rho(z) dz$$

Isostatic compensation requires that this mass be constant for all columns whatever their age. At the ridge axis the lithosphere has zero thickness, and so, taking $z = 0$ to be at sea level, the mass of the column is

$$\int_0^{d_r} \rho_w dz + \int_{d_r}^D \rho_a dz$$

where ρ_w is the density of sea water, ρ_a the density of the asthenosphere (at temperature T_a) and d_r the depth of the water over the ridge axis. The mass of a column aged t is then

$$\int_0^d \rho_w dz + \int_d^{d+L} \rho(z) dz + \int_{d+L}^D \rho_a dz$$

where d is the water depth and L the thickness of the lithosphere. Because the mass in this column must be the same as the mass in the column at the ridge axis,

we obtain the equation

$$\int_0^{d_r} \rho_w dz + \int_{d_r}^D \rho_a dz = \int_0^d \rho_w dz + \int_d^{d+L} \rho(z) dz + \int_{d+L}^D \rho_a dz \quad (7.66)$$

Rearranging yields

$$(d - d_r)(\rho_a - \rho_w) = \int_0^L (\rho(z) - \rho_a) dz \quad (7.67)$$

To determine $\rho(z)$, we must use the expression for density as a function of temperature and α the coefficient of thermal expansion,

$$\rho(T) = \rho_a[1 - \alpha(T - T_a)] \quad (7.68)$$

and Eq. (7.61) for the temperature structure of the lithosphere. Substituting these two equations into Eq. (7.67) gives

$$(d - d_r)(\rho_a - \rho_w) = \rho_a \alpha T_a \int_0^L \operatorname{erfc}\left(\frac{z}{2\sqrt{\kappa t}}\right) dz \quad (7.69)$$

where erfc is the complementary error function (see Appendix 5). The integral on the right-hand side of this equation can easily be calculated or looked up in a set of mathematical tables. However, for our purposes it is sufficient to change the upper limit of integration from L to ∞ (the error introduced by this approximation is about 5%). This integral of $\operatorname{erfc}(x)$ between $x = 0$ and infinity is $1/\sqrt{\pi}$ (Appendix 5). When this approximation is made, Eq. (7.69) becomes

$$(d - d_r)(\rho_a - \rho_w) = 2\rho_a \alpha T_a \sqrt{\frac{\kappa t}{\pi}} \quad (7.70)$$

Rearranging Eq. (7.70) gives

$$d = d_r + \frac{2\rho_a \alpha T_a}{\rho_a - \rho_w} \sqrt{\frac{\kappa t}{\pi}} \quad (7.71)$$

If we assume values for ρ_a and for ρ_w of 3.3×10^3 and $1.0 \times 10^3 \text{ kg m}^{-3}$, respectively; for α , $3 \times 10^{-5} \text{ }^\circ\text{C}^{-1}$; for κ , $10^{-6} \text{ m}^2 \text{ s}^{-1}$; for T_a , $1200 \text{ }^\circ\text{C}$; and for d_r , 2.6 km; with t in millions of years and d in kilometres, then Eq. (7.71) is

$$d = 2.6 + 0.33\sqrt{t} \quad (7.72)$$

When T_a is taken to be $1300 \text{ }^\circ\text{C}$, Eq. (7.71) is

$$d = 2.6 + 0.36\sqrt{t} \quad (7.73)$$

Such dependence of ocean depth on age is in broad agreement with the depths observed for oceanic plates less than 70 Ma old (Eq. (7.57a)). Thus, as the lithosphere moves away from the ridge axis, it cools, contracts and hence subsides. Table 7.4 gives the details of the physical parameters for oceanic-lithosphere thermal models.

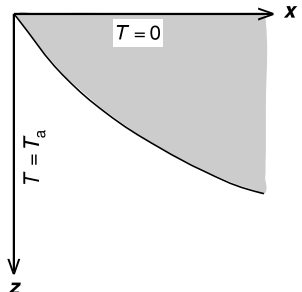
The boundary-layer or half-space models

The boundary-layer model is a modification of the simple half-space model: the rigid lithosphere is assumed to be cooled asthenosphere, and the base

Table 7.4 Thermal parameters for oceanic-lithosphere models

		GDH1	PSM	HS
L ,	plate thickness (km)	95 ± 10	125 ± 10	—
T_a ,	temperature at base of plate ($^{\circ}\text{C}$)	1450 ± 100	1350 ± 275	1365 ± 10
α ,	coefficient of thermal expansion ($^{\circ}\text{C}^{-1}$)	3.1×10^{-5}	3.28×10^{-5}	3.1×10^{-5}
k ,	thermal conductivity (W m^{-1})	3.138	3.138	3.138
c_p ,	specific heat (kJ kg^{-1})	1.171	1.171	1.171
κ ,	thermal diffusivity ($\text{m}^2 \text{s}^{-1}$)	0.804×10^{-6}	0.804×10^{-6}	0.804×10^{-6}
ρ_m ,	mantle density (kg m^{-3})	3330	3330	3330
ρ_w ,	water density (kg m^{-3})	1000	1000	1000
d_r ,	ridge depth (km)	2.6	2.5	2.6

(a) Half-space cooling models



(b) Plate model

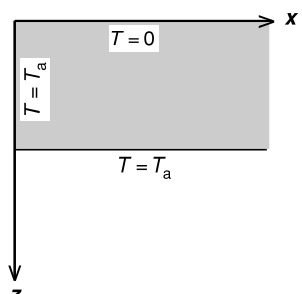


Figure 7.8. Schematic diagrams of (a) the half-space cooling and boundary-layer models and (b) the plate model of the oceanic lithosphere. Lithosphere is shaded.

Abbreviations: GDH, global depth and heat; PSM, Parsons, Sclater and McKenzie; HS, halfspace.

Sources: Stein and Stein (1992), Parsons and Sclater (1977) and Carlson and Johnson (1994).

of the lithosphere is defined by an isotherm (Fig. 7.8). The boundary condition at the base of the lithosphere is that the heat flux from the mantle is specified. The bathymetric depth predicted by these models increases as $t^{1/2}$ for all t . It is apparent from Fig. 7.7(a) that, although this model fits the observed depths out to about 60–70 Ma, for greater ages the predicted depth is too great. The heat-flow values predicted by the model decrease as $t^{-1/2}$ for all t . These predicted heat flows are close to, but lower than, the observed values (Fig. 7.7(b)). For ages greater than a few million years, the temperature and lithospheric thickness predicted by the simple model are very close to the values for the boundary-layer model.

The plate model

In the plate models, the oceanic lithosphere is taken to be of constant thickness L , the base of the lithosphere is at the same constant temperature T_a as the vertical ridge axis and the top surface of the lithosphere and the seabed is another isotherm, usually put at 0°C (Fig. 7.8). The solution to Eq. (7.59) with these boundary conditions, $T = T_a$ on $z = L$, $T = 0$ on $z = 0$ and $T = T_a$ on $t = 0$, is

$$T = T_a \left\{ \frac{z}{L} + \sum_{n=1}^{\infty} \frac{2}{n\pi} \sin\left(\frac{n\pi z}{L}\right) \exp\left[\left(\frac{uL}{2\kappa} - \sqrt{\frac{u^2 L^2}{4\kappa^2} + n^2 \pi^2}\right) \frac{ut}{L}\right] \right\} \quad (7.74)$$

When the horizontal conduction of heat is ignored, this simplifies to

$$T = T_a \left[\frac{z}{L} + \sum_{n=1}^{\infty} \frac{2}{n\pi} \sin\left(\frac{n\pi z}{L}\right) \exp\left(-\frac{n^2\pi^2\kappa t}{L^2}\right) \right]$$

A thermal time constant can be defined as $t_0 = L^2/(\pi^2\kappa)$.

The surface heat flow as a function of plate age, $Q(t)$, for this model is

$$Q(t) = \frac{kT_a}{L} \left[1 + 2 \sum_{n=1}^{\infty} \exp\left(-\frac{n^2\pi^2 t}{L^2}\right) \right]$$

The asymptotic value for the heat flow over old lithosphere is therefore kT_a/L .

The depth of the seabed as a function of plate age, $d(t)$, for this model is calculated in exactly the same way as for the simple half-space model:

$$d(t) = d_r + \frac{\rho_a \alpha T_a L}{2(\rho_a - \rho_w)} \left[1 - \frac{8}{\pi^2} \sum_{n=1}^{\infty} n^2 \left(-\frac{n^2\pi^2\kappa t}{L^2} \right) \right]$$

The asymptotic value for the ocean depth over old lithosphere is therefore

$$d_r + \frac{\rho_a \alpha T_a L}{2(\rho_a - \rho_w)}$$

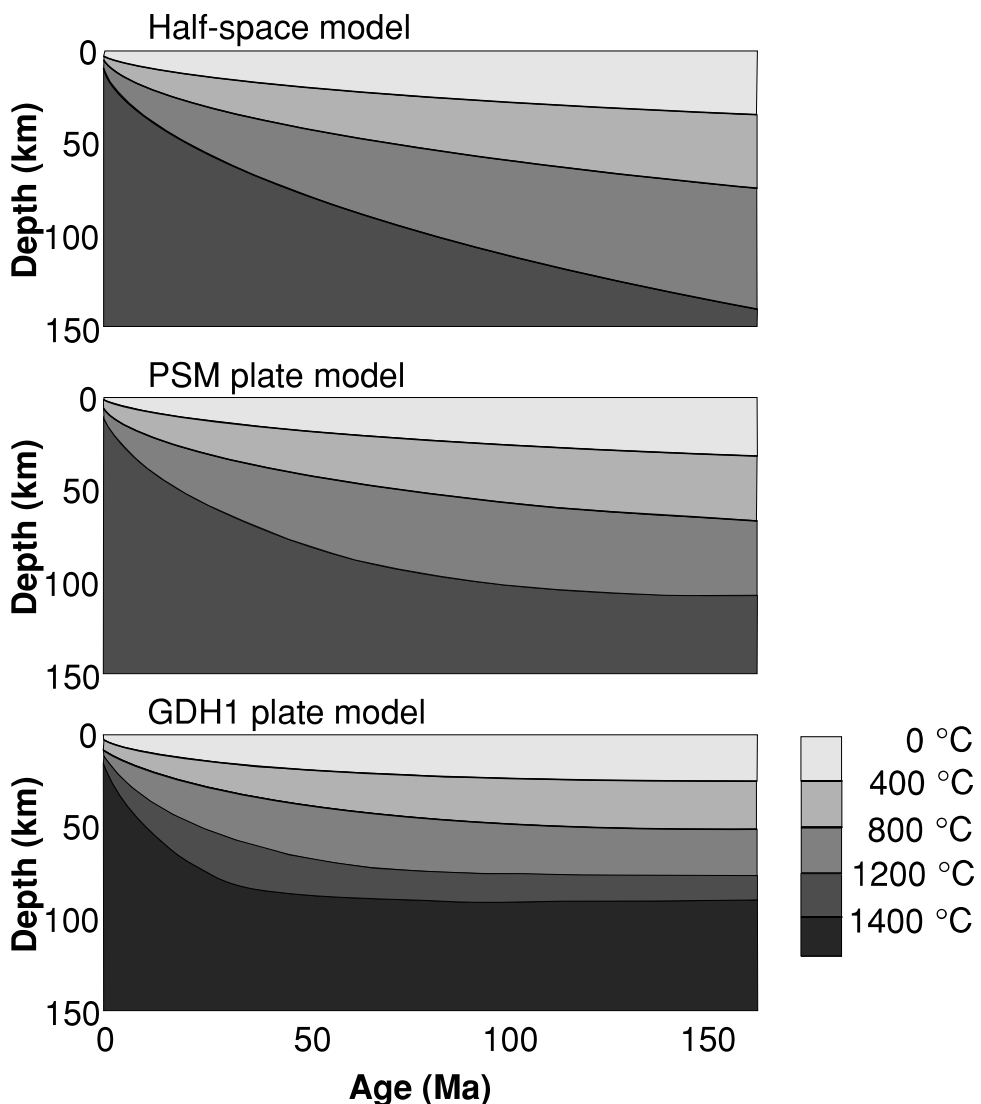
Isotherms for the two plate models, PSM and GDH1, with temperatures of 1350 and 1450 °C, respectively, at the base of the lithosphere and at the ridge axis are shown in Fig. 7.9. As the lithosphere ages and moves away from the ridge axis, the isotherms descend until, far from the ridge, they essentially reach equilibrium. Figures 7.6 and 7.7 show that the heat flow and bathymetric depths predicted by these models are in good agreement with observations. Note that there is effectively no difference between the heat flows predicted by the HS and PSM models, compared with the scatter in the data (Figs. 7.6, 7.7(b) and Table 7.5). The differences between ocean depths predicted by the plate models and by the boundary-layer model become apparent beyond about 60–70 Ma and the deviation of the ocean depth from the \sqrt{t} curve predicted by the half-space model shows up clearly in Fig. 7.7(c). Since there is no limit to how cool the upper regions of the boundary-layer model can become, there is no limit to its predicted ocean depths. The plate model has a uniformly thick lithosphere, so temperatures in the lithosphere, as well as ocean depths, predicted by that model approach equilibrium as age increases. For the same reason, differences between the surface heat flows predicted by the two types of model begin to become apparent for ages greater than about 100 Ma – the boundary-layer model keeps on cooling whereas the plate models approach equilibrium.

Any thermal model must account for the \sqrt{t} dependence of ocean depth on age for young oceanic lithosphere. Additionally the model must account for the asymptotic behaviour both of ocean depth and of heat flow on old lithosphere. The GDH1 plate model fits the whole dataset best (with the lowest residuals), but a half-space model fits the ocean-depth dataset for young lithosphere best.

Table 7.5 Variation of depth and heat flow with age for oceanic-lithosphere models

	Ocean depth (km)	Heat flow (mW m^{-2})
Half-space	$2.6 + 0.345t^{1/2}$	$480t^{-1/2}$
PSM	$2.5 + 0.350t^{1/2}, t < 70 \text{ Ma}$	$473t^{-1/2}, t < 120 \text{ Ma}$
	$6.4 - 3.2e^{-t/62.8}, t > 70 \text{ Ma}$	$33.5 + 67e^{t/62.8}, t > 120 \text{ Ma}$
GDH1	$2.6 + 0.365t^{1/2}, t < 20 \text{ Ma}$	$510t^{-1/2}, t < 55 \text{ Ma}$
	$5.65 - 2.47e^{-t/36}, t > 20 \text{ Ma}$	$49 + 96e^{-t/36}, t > 55 \text{ Ma}$

Figure 7.9. Temperature contours for three thermal models of the oceanic lithosphere. The half-space model and the plate models PSM (Parsons, Sclater and McKenzie) and GDH1 (global depth and heat) are shown schematically in Fig. 7.8. The GDH1 model has been constrained so that it fits both the oceanic depth and heat-flow measurements. Note that GDH1 has a thinner plate and higher temperatures than the other models. (After Stein and Stein, Thermo-mechanical evolution of oceanic lithosphere: implications for the subduction process and deep earthquakes (overview), Geophysical Monograph 96, 1–17, 1996. Copyright 1996 American Geophysical Union. Modified by permission of American Geophysical Union.)



The differences between the predictions of these models are small, but their values for mantle temperature and plate thickness are rather different (Table 7.4). The variability in the depth and heat-flow data resulting from hotspot proximity, mantle thermal structure and hydrothermal circulation means that it is not possible to establish an unequivocal global thermal model that can simultaneously account for all the depth and heat-flow data at every age. The variations of depth and heat flow with age for the half-space, PSM and GDH1 models are summarized in Table 7.5.

Thermal structure of the oceanic lithosphere

Both plate and boundary-layer models of the lithosphere provide heat-flow values that are in reasonable agreement with the measured values, but the ocean depths predicted by the plate model and boundary-layer models differ, with the plate-model predictions being overall in much better agreement with observed ocean depths. Other geophysical evidence on the structure of the oceanic lithosphere also shows that the oceanic lithosphere thickens with age, but they cannot distinguish amongst the thermal models (Fig. 5.17). The effective elastic thickness (determined from studies of loading and a measure of the long-term strength of the lithosphere) increases with age approximately as the 400-°C isotherm. The maximum focal depth of intraplate earthquakes (a measure of the short-term strength of the lithosphere) increases with age approximately as the 600–700-°C isotherm. Results of surface-wave-dispersion studies show that the depth to the low-velocity zone (the top of the asthenosphere) also deepens with age with plate-model isotherms. However, while all these parameters clearly increase with lithospheric age and broadly follow isotherms for the plate models, they are not well enough determined to allow one to distinguish amongst the various thermal models.

The observations could be reconciled with the boundary-layer model if some mechanism to slow the cooling of the boundary layer model for ages greater than ~70 Ma were found, so that it would resemble the plate model. Two mechanisms for maintaining the heat flux at the base of the lithosphere have been proposed: shear-stress heating caused by a differential motion between lithosphere and asthenosphere; and an increasing rate of heat production in the upper mantle. These mechanisms are both somewhat unlikely; perhaps a better proposal is that small-scale convection occurs in the asthenosphere at the base of the older lithosphere. This would increase the heat flux into the base of the rigid lithosphere and maintain a more constant lithospheric thickness.

The lithospheric plate is thought to consist of two parts: an upper rigid layer and a lower viscous thermal boundary layer (Fig. 7.10). At about 60 Ma this thermal boundary layer becomes unstable; hence small-scale convection develops within it (see Section 8.2), resulting in an increase in heat flow to the base of the rigid layer and a thermal structure similar to that predicted by the plate model. Very detailed, accurate measurements of heat flow, bathymetry and the geoid on old

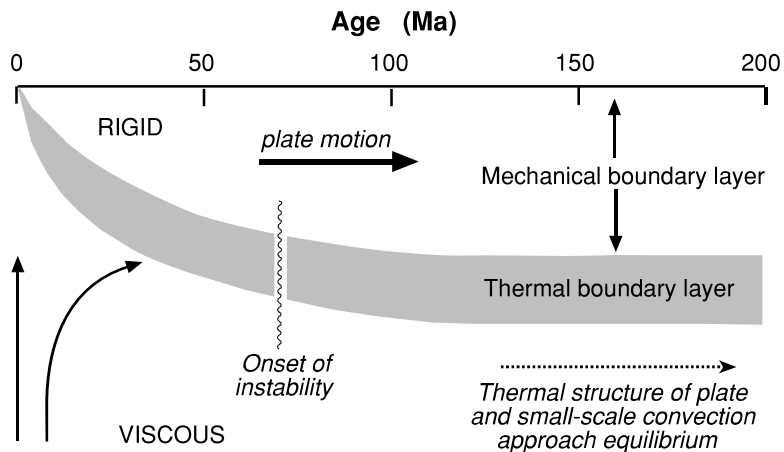


Figure 7.10. A schematic diagram of the oceanic lithosphere, showing the proposed division of the lithospheric plate. The base of the mechanical boundary layer is the isotherm chosen to represent the transition between rigid and viscous behaviour. The base of the thermal boundary layer is another isotherm, chosen to represent correctly the temperature gradient immediately beneath the base of the rigid plate. In the upper mantle beneath these boundary layers, the temperature gradient is approximately adiabatic. At about 60–70 Ma the thermal boundary layer becomes unstable, and small-scale convection starts to occur. With a mantle heat flow of about $38 \times 10^{-3} \text{ W m}^{-2}$ the equilibrium thickness of the mechanical boundary layer is approximately 90 km. (From Parsons and McKenzie (1978).)

oceanic crust and across fracture zones may improve our knowledge of the thermal structure of the lithosphere.

7.6 Continental heat flow

7.6.1 The mantle contribution to continental heat flow

Continental heat flow is harder to understand than oceanic heat flow and harder to fit into a general theory of thermal evolution of the continents or of the Earth. Continental heat-flow values are affected by many factors, including erosion, deposition, glaciation, the length of time since any tectonic events, local concentrations of heat-generating elements in the crust, the presence or absence of aquifers and the drilling of the hole in which the measurements were made. Nevertheless, it is clear that the measured heat-flow values decrease with increasing age (Fig. 7.11). This suggests that, like the oceanic lithosphere, the continental lithosphere is cooling and slowly thickening with time. The mean surface heat flow for the continents is $\sim 65 \text{ mW m}^{-2}$. The mean surface heat flow in non-reactivated Archaean cratons is $41 \pm 11 \text{ mW m}^{-2}$, which is significantly lower than the mean value of $55 \pm 17 \text{ mW m}^{-2}$ for stable Proterozoic crust well away from Archaean craton boundaries.

That all erosional, depositional, tectonic and magmatic processes occurring in the continental crust affect the measured surface heat-flow values is shown in

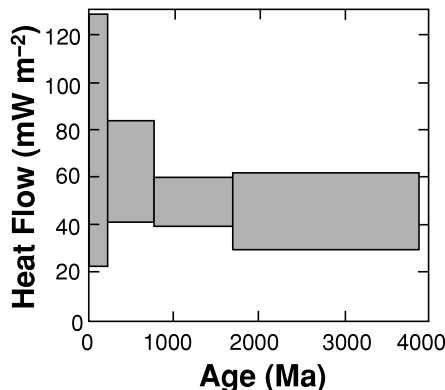


Figure 7.11. Heat flow versus crustal age for the continents. The heights of the boxes indicate the standard deviation about the mean heat flow, and the widths indicate the age ranges. (After Sclater *et al.* (1980).)

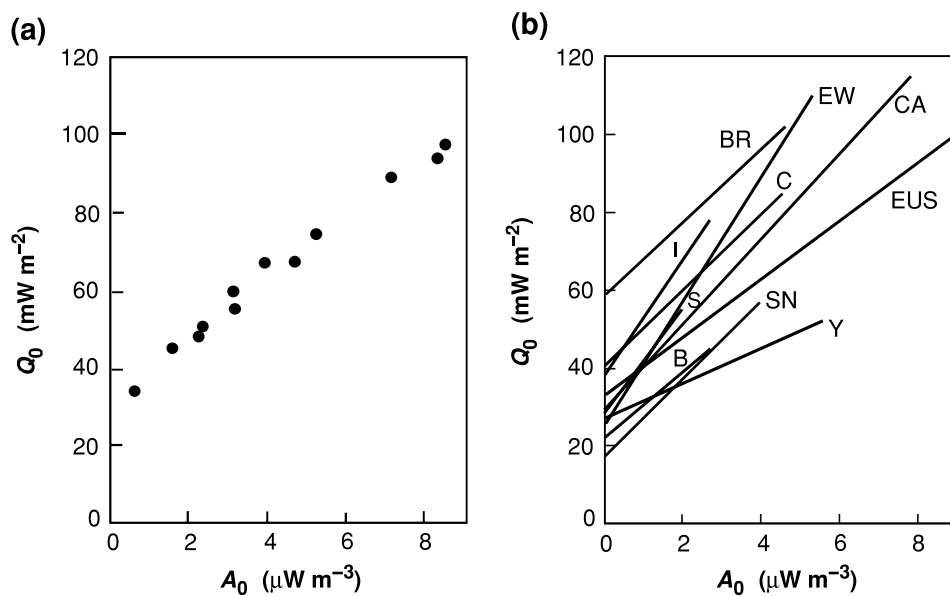


Figure 7.12. Measured heat flow Q_0 plotted against internal heat generation A_0 for (a) the eastern-U.S.A. heat-flow province. The straight line $Q_0 = Q_r + DA_0$ that can be fitted to these measurements has $Q_r = 33 \times 10^{-3} \text{ W m}^{-2}$ and $D = 7.5 \text{ km}$. (After Roy *et al.* (1968).) (b) Best-fitting straight lines for other heat-flow provinces: CA, central Australia; B, Baltic shield; BR, Basin and Range; C, Atlantic Canada; EW, England and Wales; EUS, eastern USA; I, India; S, Superior Province; SN, Sierra Nevada; and Y, Yilgarn block, Australia. (After Jessop (1990).)

the examples of Sections 7.3 and 7.8. The particularly scattered heat-flow values measured at ages less than about 800 Ma are evidence of strong influence of these transient processes and are therefore very difficult to interpret in terms of the deeper thermal structure of the continents.

In some specific areas known as heat-flow provinces, there is a linear relationship between surface heat flow and surface radioactive heat generation (Fig. 7.12). Using this relationship, one can make an approximate estimate of the contribution of the heat-generating elements in the continental crust to the surface heat flow. In these heat-flow provinces, some of which are listed in Table 7.6, the surface heat flow Q_0 can be expressed in terms of the measured surface radioactive heat generation A_0 as

$$Q_0 = Q_r + A_0 D \quad (7.75)$$

where Q_r and D are constants for each heat-flow province.

Table 7.6 Some continental heat-flow provinces

Province	Mean Q_0 (10^{-3} W m $^{-2}$)	Q_r (10^{-3} W m $^{-2}$)	D (km)
Basin and Range (U.S.A.)	92	59	9.4
Sierra Nevada (U.S.A.)	39	17	10.1
Eastern U.S.A.	57	33	7.5
Superior Province (Canadian Shield)	39	21	14.4
U.K.	59	24	16.0
Western Australia	39	26	4.5
Central Australia	83	27	11.1
Ukrainian Shield	37	25	7.1

Source: Sclater *et al.* (1980).

We consider here two extreme models of the distribution of the radioactive heat generation in the crust, both of which yield a surface heat flow in agreement with this observed linear observation.

1. *Heat generation is uniformly concentrated within a slab with thickness D .* In this case, using Eq. (7.16), we obtain

$$\frac{\partial^2 T}{\partial z^2} = -\frac{A_0}{k} \quad \text{for } 0 \leq z \leq D$$

Integrating once gives

$$\frac{\partial T}{\partial z} = -\frac{A_0}{k}z + c \quad (7.76)$$

where c is the constant of integration. At the surface, $z = 0$, the upward heat flow $Q(0)$ is

$$\begin{aligned} Q(0) &= Q_0 = k \left. \frac{\partial T}{\partial z} \right|_{z=0} \\ &= kc \end{aligned} \quad (7.77)$$

Therefore, the constant c is given by

$$c = \frac{Q_0}{k}$$

At depth D , the upward heat flow is

$$\begin{aligned} Q(D) &= k \left(-\frac{A_0 D}{k} + \frac{Q_0}{k} \right) \\ &= -A_0 D + Q_0 \\ &= Q_r \end{aligned} \quad (7.78)$$

Thus, in this case, the heat flow $Q(D)$ into the base of the uniform slab (and the base of the crust, since all the heat generation is assumed to be concentrated in the slab) is the Q_r of Eq. (7.75).

2. Heat generation is an exponentially decreasing function of depth within a slab of thickness z^* . Equation (7.16) then becomes

$$\frac{\partial^2 T}{\partial z^2} = -\frac{A(z)}{k} \quad (7.79)$$

where

$$A(z) = A_0 e^{-z/D} \quad \text{for } 0 \leq z \leq z^*$$

Integrating Eq. (7.79) once gives

$$\frac{\partial T}{\partial z} = \frac{A_0}{k} D e^{-z/D} + c \quad (7.80)$$

where c is the constant of integration. At the surface, $z = 0$, the heat flow is $Q(0)$

$$\begin{aligned} Q(0) &= Q_0 = k \left(\frac{A_0 D}{k} + c \right) \\ &= A_0 D + kc \end{aligned} \quad (7.81)$$

The constant c is given by

$$c = \frac{Q_0 - A_0 D}{k} \quad (7.82)$$

At depth z^* (which need not be uniform throughout the heat-flow province), the heat flow is

$$\begin{aligned} Q(z^*) &= k \left(\frac{A_0 D}{k} e^{-z^*/D} + \frac{Q_0 - A_0 D}{k} \right) \\ &= A_0 D e^{-z^*/D} + Q_0 - A_0 D \end{aligned} \quad (7.83)$$

Thus, by rearranging, we obtain

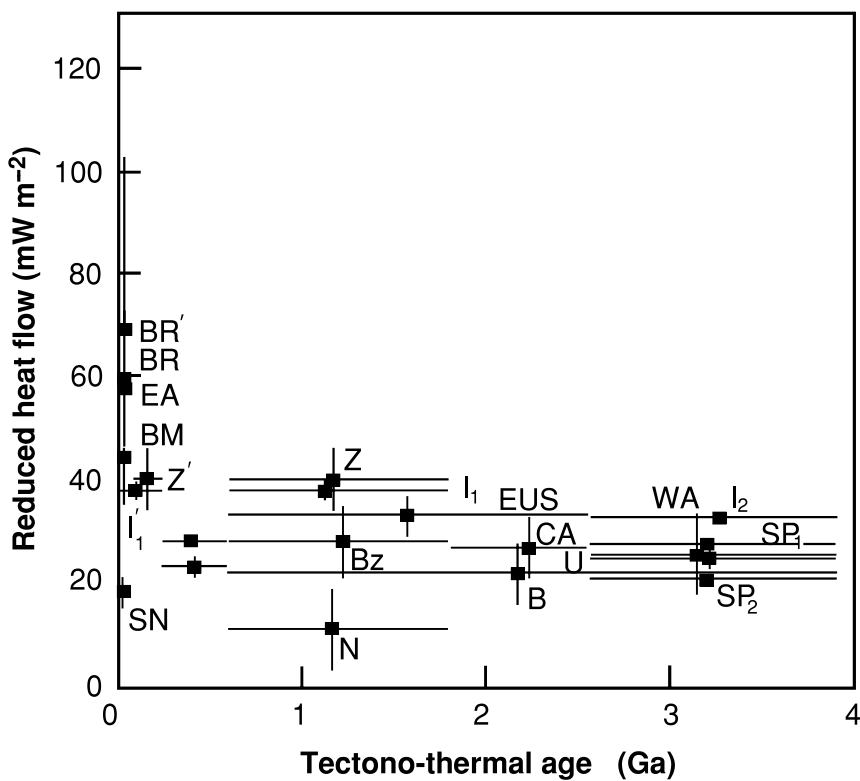
$$Q_0 = Q(z^*) + A_0 D - A_0 D e^{-z^*/D} \quad (7.84)$$

Equation (7.84) is the same as Eq. (7.75) if we write

$$\begin{aligned} Q_r &= Q(z^*) - A_0 D e^{-z^*/D} \\ &= Q(z^*) - A(z^*) D \end{aligned} \quad (7.85)$$

Thus, the linear relation is valid for this model if the heat generation $A(z^*)$ at depth z^* is constant throughout the heat-flow province. Unless $A(z^*)D$ is small, the observed value of Q_r may be very different from the actual heat flow $Q(z^*)$ into the base of the layer of thickness z^* . However, it can be shown (for details see Lachenbruch (1970) that, for some heat-flow provinces, $A(z^*)D$ is small, and thus Q_r is a reasonable estimate of $Q(z^*)$). This removes the constraint that $A(z^*)$ must be the same throughout the heat-flow province. Additionally, for those provinces in which $A(z^*)D$ is small, it can be shown that z^* must be substantially greater than D . Thus, the exponential distribution of heat production satisfies the observed linear relationship between surface heat flow and heat generation and does so even in cases of differential erosion. In this model, D is a measure of the upward migration of the heat-producing radioactive isotopes (which can be justified on geochemical grounds), and Q_r is approximately the heat flow into

Figure 7.13. Reduced heat flow Q_r versus time since the last tectono-thermal event for the continental heat flow provinces. The error bars represent the uncertainties in the data. The solid lines show the reduced heat flows predicted by the plate model. BR and BR', Basin and Range; SEA, southeast Appalachians; SN, Sierra Nevada; EUS, eastern U.S.A.; SP₁ and SP₂, Superior Province; Bz, Brazilian coastal shield; B, Baltic shield; BM, Bohemian massif; U, the Ukraine; EW, England and Wales; N, Niger; Z and Z', Zambia; WA, western Australia; CA, central Australia; EA, eastern Australia; I₁ and I'₁, Indian shield; and I₂, Archaean Indian shield. (After Morgan (1984) and Stein (1995), *Heat Flow of the Earth*, AGU Reference Shelf 1, 144–58, 1995. Copyright 1995 American Geophysical Union. Modified by permission of American Geophysical Union.)



the base of the crust (because z^* is probably approximately the thickness of the crust).

Neither of these models of the distribution of heat generation within the crust allows for different vertical distributions among the various radioactive isotopes. There is some evidence for such variation. Nevertheless, it is clear that much of the variation in measured surface heat flow is caused by the radioactive heat generation in the crust and that the reduced heat flow Q_r is a reasonable estimate of the heat flow into the base of the crust. Figure 7.13 shows this reduced heat flow plotted against age. After about 300 Ma since the last tectonic/thermal event, the reduced heat flow exhibits no variation and attains a value of $(25 \pm 8) \times 10^{-3} \text{ W m}^{-2}$. This is within experimental error of the value predicted by the plate model of the oceanic lithosphere and suggests that there should be no significant difference between models of the thermal structures of the oceanic and continental lithospheres. The present-day thermal differences are primarily a consequence of the age disparity between oceanic and continental lithospheres.

7.6.2 The temperature structure of the continental lithosphere

Figure 7.14 shows two extreme temperature models of the equilibrium oceanic lithosphere, O₁ and O₂, and two extreme models of the old stable continental

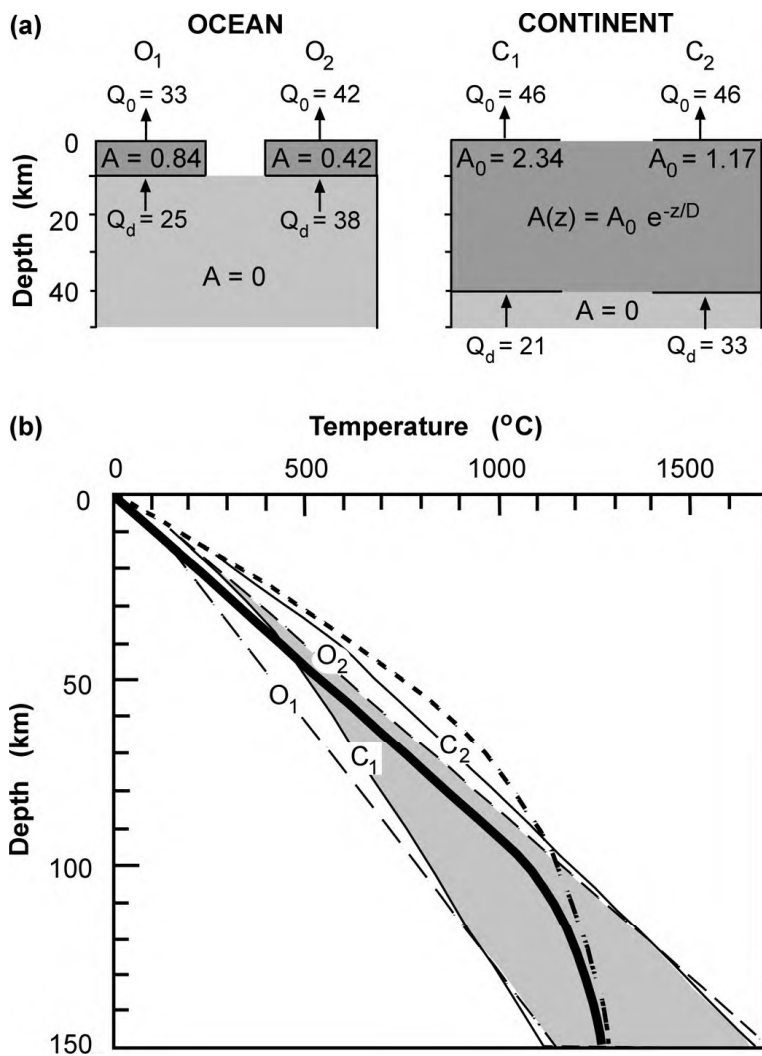


Figure 7.14. (a) Extreme thermal models used to calculate equilibrium geotherms beneath an ocean, O_1 and O_2 , and beneath an old stable continent, C_1 and C_2 . Heat flows Q_0 and Q_d are in mW m^{-2} ; heat generation A_0 is in $\mu\text{W m}^{-3}$. (b) Predicted geotherms for these models. Thin dashed lines, oceanic geotherms; thin solid lines, continental geotherms; heavy solid line, equilibrium geotherm for the PSM plate model, taking into account the small-scale convection occurring in the thermal boundary layer (see Fig. 7.10). Grey shading, region of overlap. The heavy dashed line is an error function for the geotherm of age 70 Ma (see Section 7.5.2). The mantle temperature T_a is taken as 1300 $^{\circ}\text{C}$. (After Parsons and McKenzie (1978) and Sclater *et al.* (1981b).)

lithosphere, C_1 and C_2 . These have been calculated by using the one-dimensional heat-conduction equation. The extensive region of overlap of these four geotherms indicates that, on the basis of surface measurements, for depths greater than about 80 km there need be little difference in equilibrium temperature structure beneath oceans and continents. All the proposed oceanic thermal models (Section 7.5) fall within the shaded region of overlap. The solid line is the geotherm for the oceanic-plate model in Fig. 7.10. The heavy dashed line is the geotherm for the simple error-function model of Section 7.5.2. Figure 7.15 shows thermal models of oceanic and old continental lithospheres.

7.7 The adiabat and melting in the mantle

The previous sections have dealt in some detail with the temperatures in the continental and oceanic lithosphere and with attempts to estimate the temperatures in the mantle and core, assuming that heat is transferred by conduction. For the